Trans. Tianjin Univ. 2015, 21: 250-258
DOI 10.1007/s12209-015-2408-x

CFD Prediction of Mean Flow Field and Impeller Capacity for Pitched Blade Turbine

Qiao Shengchao(乔胜超), Wang Rijie(王日杰), Yang Xiaoxia(杨晓霞),
Yan Yuefei(闫越飞)
(School of Chemical Engineering and Technology, Tianjin University, Tianjin 300072, China)

Abstract: This work focused on exploring a computational fluid dynamics (CFD) method to predict the macro-mixing characteristics including the mean flow field and impeller capacity for a 45° down-pumping pitched blade turbine (PBT) in stirred tanks. Firstly, the three typical mean flow fields were investigated by virtue of three components of liquid velocity. Then the effects of impeller diameter (D) and off-bottom clearance (C) on both the mean flow field and three global macro-mixing parameters concerning impeller capacity were studied in detail. The changes of flow patterns with increasing C/D were predicted from these effects. The simulation results are consistent with the experimental results in published literature.

Keywords: CFD simulation; PBT; stirred tank; flow field; pumping capacity

The pitched blade turbine (PBT) is considered to be a kind of simple and versatile impeller for mechanical agitations in both laboratorial and industrial reactors, since it has a good balance between the pumping and shear capability. PBT (especially down-pumping mode) is widely used in practical applications involving the immiscible liquid mixing, gas dispersion and solid suspension[1-3]. Mechanical mixing achieved through both bulk convection and turbulent diffusion is distinguished into macro-mixing (mixing at the bulk scale of the tank) and micro-mixing (mixing at the molecular scale). However, micro-mixing performance is usually dominated by macro-mixing[4]. To improve the mixing quality and optimize the impeller design, the macro-mixing characteristics, such as the liquid velocity distribution and pumping capacity should be well understood.

Three global macro-mixing parameters, including power number (N_p), pumping number (N_q) and pumping effectiveness (η_e), largely depend on the mean flow fields or flow patterns, which are strongly affected by many impeller design variables[5]. Some qualitative or quantitative results of the mean flow fields produced by PBT impeller and the dependence on some key design variables, especially D and C, were reported in published literature[6-9]. These studies were usually preformed by the experimental fluid dynamics (EFD) method. Information about the velocity field or turbulent flow is difficult to be obtained by using EFD method, unless by using some complex and expensive instruments such as laser Doppler anemometry (LDA).

Tremendous progress has been made in CFD method in past decades, and it has been promoted as a powerful tool to predict fluid flow and model various geometries in stirred tanks. Numerical simulation based on the Reynolds-averaged Navier-Stokes (RANS) equation is the most widespread CFD method to provide quantitative or qualitative information about the velocity field and turbulent field[10, 11]. Effects of many numerical issues on the RANS-based prediction of turbulent flow in the stirred tanks were investigated in published literature[12-14], and these works indicated that RANS simulation along with the impeller rotation model of multiple reference frame (MRF) and the k-ε turbulence model could reasonably simulate both the mean flow fields and turbulence. Generally, more satisfactory agreements between simulated and experimental data have been reported for the large eddy simulation (LES) relative to RANS simulation, but at cost of much larger computational requirement and numerical effort[14]. Besides, Deglon and Meyer[13] reported that the underestimate of turbulence obtained by k-ε turbulence model in RANS simulation was found to be attributed to the numerical errors

Accepted date: 2014-05-19.
Qiao Shengchao, born in 1986, male, doctorate student.
Correspondence to Wang Rijie, E-mail: rjwtju@163.com.

rather than inadequacies in the turbulence model, which was at variance with many other papers. The numerical errors in modeling turbulence could be well eliminated in the condition when fine enough grids coupled with higher-order discretization schemes were used.

An extensive survey of recent literature shows that there are few CFD studies on the mean flow fields, especially on the impeller capacity of PBT[15]. In view of the potentials of CFD method, therefore, RANS simulation was performed in this work to further understand the mean flow fields and predict flow patterns produced by a down-pumping PBT impeller in a stirred tank used by Kresta and Wood[8]. Additionally, the influences of two key design variables D and C on the mean flow fields, especially on three global macro-mixing parameters, have not been reported. Thus, RANS simulations coupled with k-ε turbulence model were adopted to study these effects in detail and the transition or change of flow patterns with increasing C/D was predicted as well.

1 CFD simulation

1.1 Model and method

The Reynolds-averaged continuity and momentum equations for an incompressible fluid were solved to describe the turbulent motion. Numerical solutions of these governing equations were achieved by using CFD software Fluent 6.3. As for the turbulence closure, the three extensions of k-ε turbulence model (standard, RNG and realizable k-ε model[16]) were compared. Predicted results showed no significant differences in the three models, and thus realizable k-ε turbulence model was adopted in this research. The SIMPLEC algorithm was used to couple the pressure and velocity fields. Three discretization schemes, first-order upwind, second-order upwind and higher order QUICK schemes for the convective terms of momentum, k and ε equations were compared[17]. The mass integral of ε increased with the improvement of the scheme order, but the difference between second-order and QUICK schemes was not significant. Hence, QUICK scheme with the highest precision was used in this study.

1.2 System and solution domain

An experimental setup used by Kresta and Wood[8] was considered for comparison and validation. The investigated system was a flat-bottomed cylindrical tank with diameter $T = 0.152\,4$ m. Four full baffles with the width of $1/10T$ were symmetrically mounted perpendicular to the wall. The investigated impeller was a 4-bladed PBT of $W = D/5$ in width and $t = 0.8$ mm in thickness, which was inclined at 45^{o} to the horizontal. Four blades were fixed on the hub with the outer and inner diameter of 12.7 and 6.35 mm, respectively. The impellers with the diameter D of $T/3$ and $T/2$ were studied with the dimensionless off-bottom clearances C/D of 0.155—2.1 and 0.25—1.43. The water with the density of $\rho_l = 996$ kg/m^3 and the viscosity of $\mu_l = 1 \times 10^{-3}$ Pa·s was simulated as the test fluid and filled in the tank with the liquid height $H = T$. Considering the symmetry of the solution domain, only one quarter was modeled to reduce the computational requirement and numerical effort.

The simulated results of the mean flow fields were quantitatively compared with the experimental data of Kresta and Wood[8] from their flow visualization or LDA experiments. They reported EFD results in the form of three components of liquid velocity over the radial traverses at seven axial positions below the impeller. Simulated results of the turbulent flow fields were not presented in this study also due to the lack of the experimental data.

The origin was defined at the center of lower blade edge with z defined to be positive upward and r to be positive outward. The dimensionless distances ($2z/W$) from the origin to seven traverses A—I are displayed in Fig. 1. Specifics of three representative cases or configurations are listed in Tab. 1.

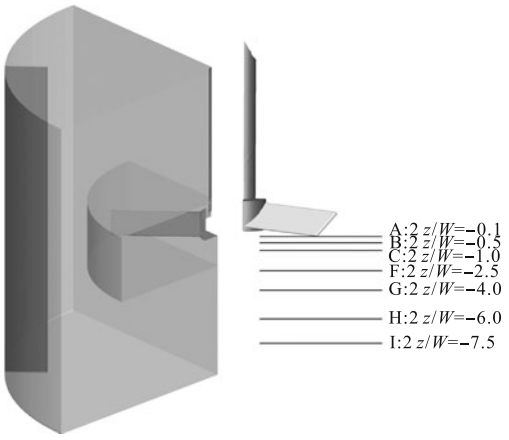

Fig. 1 Tank geometry and seven traverses below impeller

The MRF approach was used to model the relative motion between the rotating impeller and stationary baffle. Initial simulations performed with the transient sliding mesh (SM) model obtained only slightly improved results. For example, the difference of N_p predicted by these two impeller rotation models was less than 5%. In MRF approach, the solution domain was mainly divided into two reference frames: rotating and stationary refer-

ence frames. The rotating reference frame was a cylinder region encompassing the impeller and discharge stream surrounding it. The diameter and height of this cylinder region were $0.6T$ and $3W$, respectively. The stationary reference frame contained the remaining domains. This frame was further divided into three sub-regions and then meshed with hexahedral grid cells by a grid generation tool, Gambit. The tetrahedral grid cells with finer resolution were applied to mesh the irregular cylinder region to ensure the adequate estimation of turbulent quantities produced by the impeller. Grid-sensitivity study was performed in the preliminary simulations.

Tab. 1 CFD simulations of three typical cases

	C/mm	D	C/D	N/(r·s^{-1})	Re	Flow regime
Case 1	70.8	$T/2$	0.93	7.5	43 374	Turbulent
Case 2	47.2	$T/3$	0.93	7.5	19 277	Turbulent
Case 3	38.1	$T/2$	0.50	6.7	38 748	Turbulent

1.3 Boundary condition

The 'periodic' boundary condition was used for the left and right halves of the symmetry plane. The distortion of free liquid surface (gas-liquid interface) was beyond the scope of this research since its effect was negligible in the fully baffled tanks. For single baffle cases, a more accurate treatment of free surface was required to predict the turbulence and transient eddies at the surface, but for full baffle cases, this approximation was reasonable[18]. Hence, the 'symmetry' boundary condition with zero normal velocity gradients was imposed on the free liquid surface. The 'no-slip' boundary condition coupled with standard wall function was used for the tank wall, as well as the surfaces of shaft, blades and baffles. The interfaces between the impeller region and its adjacent region were modeled with the 'interface' boundary condition.

1.4 Impeller capacity

A useful index for characterizing the impeller capacity is the pumping effectiveness (η_e)[5], which means the pumping rate of the impeller per unit power consumption and is defined as

$$\eta_e = N_q / N_p \tag{1}$$

$$N_p = P / \rho N^3 D^5 \tag{2}$$

$$N_q = Q / ND^3 \tag{3}$$

where power number N_p is the dimensionless form of power consumption P ($P = 2\pi NM$). N_p could be calculated with the torque M derived from the pressure and tangential stress on the blade surfaces or from the mass integral of ε for the whole solution domain. The latter was found to be small, and thus the torque method was adopted to calculate N_p in this study. For PBT impeller, the radial flow is usually dominated by more obvious axial flow, which is mainly responsible for the bulk flow and solid mixing in stirred tanks[19]. The dimensionless form of volume rate (Q_z) for the axial down-flow discharged from a down-pumping PBT impeller is considered as primary pumping number (N_{qp}), which is also an important parameter in the design of stirred tanks[9].

$$Q_z = \int V_z \mathrm{d}A_z \tag{4}$$

where V_z is the axial liquid velocity; and the axial integral region (A_z) is a circular surface below the lower blade edge with the same diameter as D.

1.5 Convergence condition

The time step was set to be 0.001 s and the transient calculations reached convergence when the total residuals for all equations, especially for the continuity equation, dropped below 10^{-5}. Further verifications of the convergence were made by observing whether the mass integral of ε for the whole solution domain remained constant.

2 Results and discussion

2.1 Grid-independence study

Preliminary simulations were firstly performed to study the sensitivity of the mean flow fields to the grid size from 1 million to 5 million computational cells. Comparisons of every two consecutive cases at an interval of around 1 million indicated that the difference in values of calculated N_p and N_{qp} between two cases decreased with the grid refinement, but the corresponding computation time increased. A grid size around 2.8 million computational cells was finally selected due to its good compromise between the accuracy and computation time. The difference of N_p and N_{qp} between the 2.8 million grids and the finest 5 million grids was less than 5%, and two simulated flow fields were basically the same. In this work, moreover, it was found that the trends of three macro-mixing parameters, rather than their specific values, were most important to predict the transition of the mean flow fields with increasing C/D.

2.2 Mean flow field

For the mean flow fields produced by a down-pumping PBT in stirred tanks, we focused on the impeller discharge stream below the impeller, where the energy input to the flow fields and the steepest velocity gradients occur. Reasonable comparisons between different configurations were conducted based on the definition of seven radial traverses in terms of projected half-blade width ($W/2$), giving an equivalent dimensionless distance from the impeller.

The first two representative configurations in Tab. 1 were simulated. Good agreements were achieved between EFD and CFD results. The axial component of liquid velocity (V_z) along the lower edge of blade was considered firstly (Fig. 2 (a), Fig. 3 (a)), since this component was mainly responsible for the bulk flow in stirred tanks. Both configurations show an increasing-decreasing behavior with the smooth peaks between $2r/D = 0.7$ and 0.9, around 50% of the blade tip speed (V_{tip}). The decay of V_z begins from impeller to tank bottom with relatively small change between the traverse A and C, i.e., $2z/W = -0.1$ — -1.0. As the traverses approach to the bottom, however, some striking differences between two configurations are found. For Case 1 (Fig. 2), the flow reversal begins at $2z/W = -4.0$ (traverse G) with a transition of velocity magnitude from positive to negative, and the complete flow reversal emerges at the traverse H or I. While for Case 2 (Fig. 3), no obvious flow reversal is found even at the lowest traverse H ($2z/W = -6.0$). For the traverses of Case 2, additionally, V_z tends to flat off at a low level of $1.2 < 2r/D < 2.0$, as it may lie in the eye of the circulation loop with a radial width of $0.4D$.

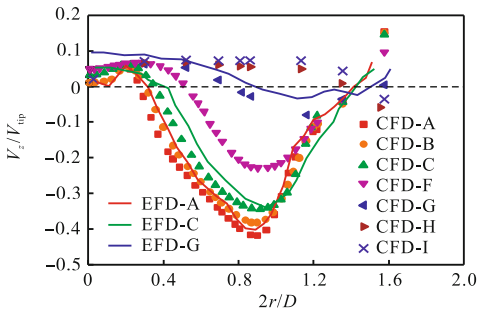

(a) Axial component

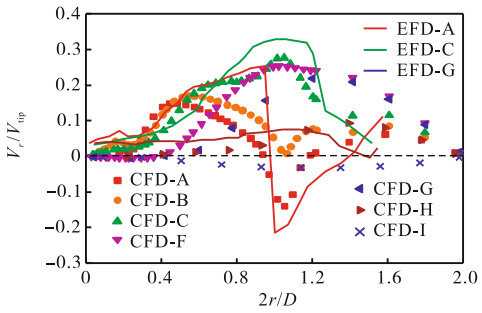

(b) Radial component

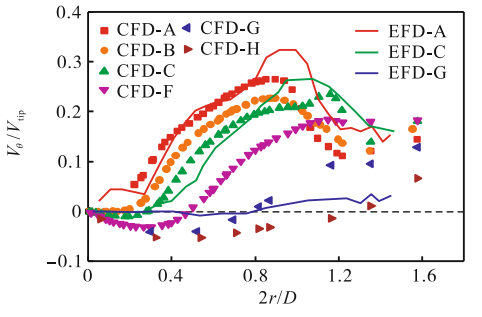

(c) Tangential component

Fig. 2 Decay of velocity profiles below impeller for Case 1

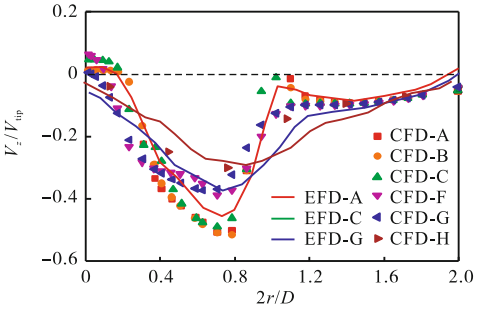

(a) Axial component

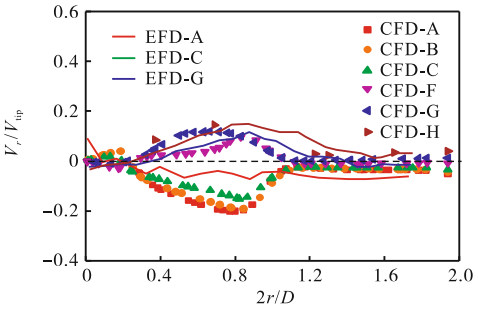

(b) Radial component

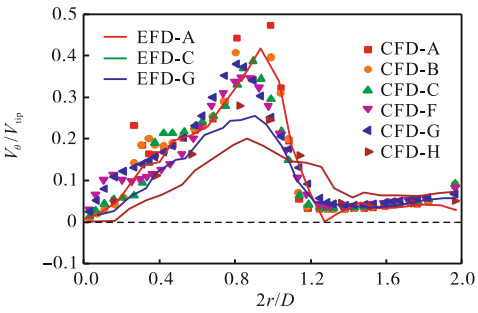

(c) Tangential component

Fig. 3 Decay of velocity profiles below impeller for Case 2

Further verification of differences between two cases was made based on the predicted contours of V_z (Fig. 4). For Case 1, in addition to a primary circulation above the impeller, a secondary circulation loop with relatively low velocity and turbulence is produced in the

form of a cone-shaped region below the impeller at the center of the tank. This flow pattern is called the 'double-eight' pattern. While for Case 2, the impeller discharge stream hits the bottom and turns predominantly upward along the wall to the top half of the tank. Only a single circulation fills the entire tank. Such a flow pattern is called 'single-eight' pattern. For both Case 1 and 2, most of the upward flow returns to the impeller region through its top surface after a long 'inverted-U' turn above the impeller.

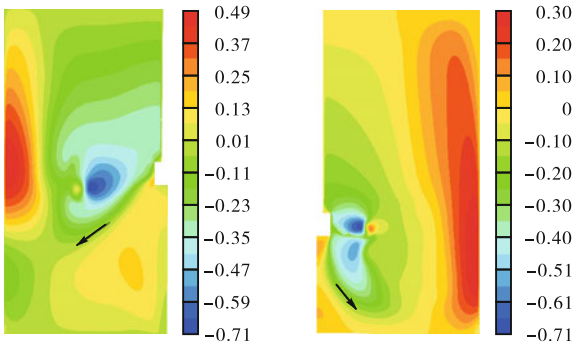

(a) Case 1 (b) Case 2

Fig. 4 Contours of predicted V_z

Profiles of the dimensionless radial velocity (V_r/V_{tip}) for two typical cases are shown in Fig. 2(b) and Fig. 3(b). Case 2 shows radial-inward flows at the traverses A—C close to the impeller. This may be caused by some short but strong circuits returning to the impeller through the vertical periphery of the impeller swept region, which can be seen from the contours of V_r (Fig. 5). The decay of V_r begins from the traverse A to F, where the flow becomes radially outward and then increases again. It implies that only a circulation loop forms in this configuration and its eye lies between the traverse C and F with an axial width of $0.75W$.

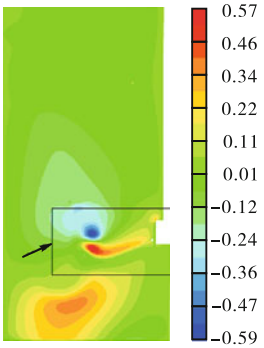

Fig. 5 Contours of predicted V_r for Case 2

Case 1 shows an entirely different result for V_r distribution. The flow along the lower blade edge (traverse A) moves radially outwards but reverses near the blade tip ($2r/D = 1.0$), which also indicates that some short circuits exist. As the traverses approach to the bottom, V_r increases steadily but begins to drop off at the traverse C. V_r shows a complete reversal radial flow over the traverse I, which was not reported in the experiment of Kresta and Wood[8], because the experiment measurement could not extend far enough in the tank.

The tangential component of velocity (V_θ) for the traverses close to the lower blade edge, shown in Fig. 2(c) and 3(c), increases to a maximum and then decays with the peak close to the blade tip in two cases. As the traverses approach to the bottom, the decay becomes smooth and steady, and the differences between two cases begin to appear. As for Case 1, the reversal of tangential flow forms over the traverses G and H, which can be attributed to the secondary loop near the bottom. While for Case 2, no reverse flow occurs and V_θ keeps at a low level from $2r/D = 1.3$ to the wall as it is in the eye of the loop, which has been found from V_z profiles.

The comparisons of results show two remarkably different flow fields and the presence of secondary circulation loop in specific configurations. Moreover, the changes of the flow fields or flow patterns may depend much on D and C.

To examine the top half of flow field in stirred tanks, the profiles of V_z above the impeller were established at seven traverses ($2z/W = 2.5$—19) for Case 3, in which C/D is smaller than that of Case 2 and thus only a strong circulation loop forms in the tank. It is found from Fig. 6 that the primary circulation loop extends over four lower traverses, which indicates that the circulation loop

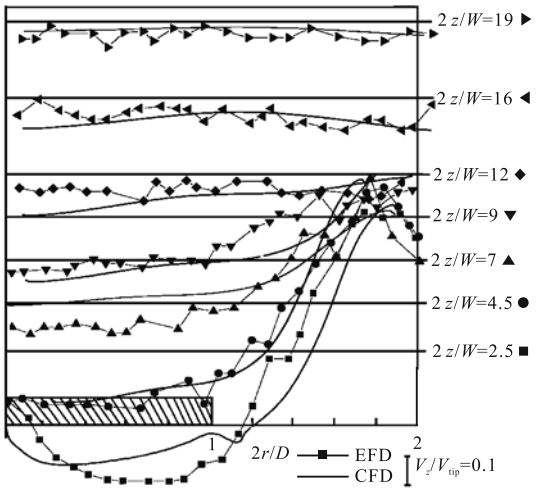

Fig. 6 Profiles of V_z in the upper portion of the tank for Case 3

begins to return to the impeller region at the height of $2z/W = 9$. While at the higher position of $2z/W = 12$, V_z begins to maintain at a low level within a narrow range. Hence the primary circulation loop covers about 65% of the whole tank.

2.3 Impeller discharge condition

CFD simulations were performed to further study the effects of D and C on the mean flow fields and flow patterns. Two impellers of $D = T/2$ and $T/3$ were positioned at different dimensionless clearances in terms of C/D to allow a reasonable comparison.

$T/3$ impeller was firstly modeled for C/D from 0.155 to 2.10, and all V_z profiles were made at the traverse B. It is found that a characteristic axial velocity profile occurs over a range of C/D in Fig. 7. Fig. 7(a) shows the profiles for high clearance conditions of C/D from 1.43 to 2.10. The profiles collapse onto single curves for $C/D = 1.62$ and 1.80. While at a higher or lower clearance, the profiles change strikingly as the peaks move radially inward and the corresponding maxima increase. The variations of profiles from $C/D = 0.75$ to 1.43 and 0.50 to 0.59 are almost the same in Fig. 7(b) and 7(c). The latter persists over a narrower range of C/D. To observe the variations of V_z from high to low clearance, profiles for $C/D = 0.93$ and 0.50 are also shown together with the lowest $C/D =$ 0.25 and 0.155 in Fig. 7(d). As the traverses approach to the bottom, the peaks move radially outward and the corresponding maxima decrease. The profiles change significantly for C/D below 0.50, since the mean flow field is strongly affected by the proximity to the tank bottom.

For $T/3$ impeller, therefore, the "single-eight" pattern forms at smaller C/D and a transition to the "double-eight" pattern occurs at $C/D = 1.43$. Then the flow fields have no significant changes at $1.62 < C/D < 1.80$. However, V_z profiles and flow fields change again due to the impacts of top surface on the bulk flow as C/D increases to 2.10.

The profiles of V_z for $T/2$ impeller at varied clearances ($C/D = 0.25$—1.43) give a similar conclusion. Two characteristic curves are found in Fig. 8(a) and (b) for high and low clearance conditions. The lowest traverse at $C/D = 0.25$ is combined in Fig. 8(c). The profile for high clearance conditions resembles that for $C/D = 0.25$ and the peak velocity achieves the highest level at low clearance conditions. Unlike $T/3$ impeller, the peak starts radially inward and then outward as C/D decreases. Moreover, the transition of the flow patterns may occur when $C/D = 0.75$.

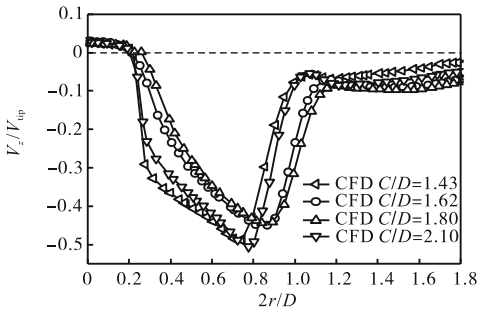

(a) C/D = 1.43 to 2.10

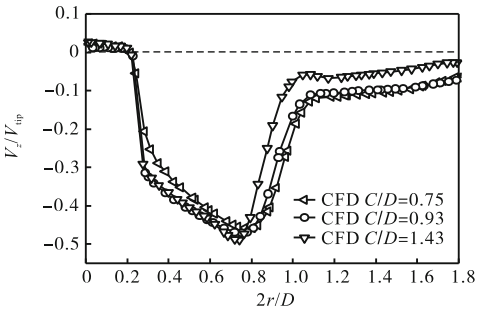

(b) C/D = 0.75 to 1.43

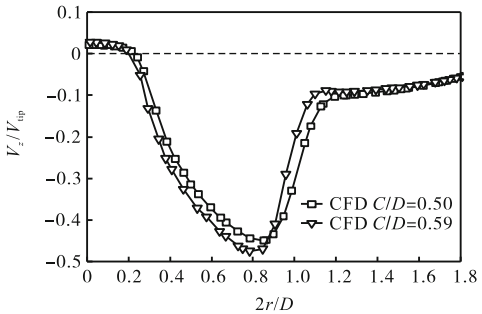

(c) C/D = 0.50 to 0.59

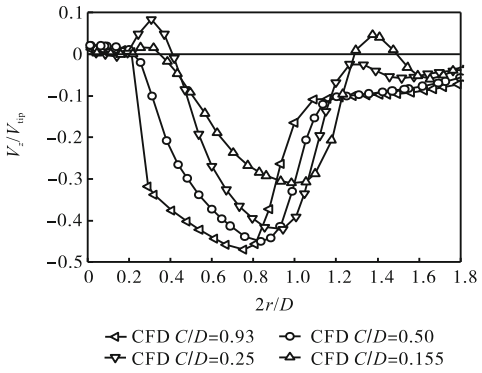

(d) Combined results

Fig. 7 Impeller discharge conditions for *T*/3 impeller

In conclusion, for $T/3$ and $T/2$ impeller, the values of C/D at which the flow pattern changes are around 1.43 and 0.75, respectively. All characteristic profiles are shown in Fig. 9 to make comparisons between two impellers. It is firstly noted that as the clearance increases, the reverse flow of the secondary loop near the bottom de-

flects the impeller discharge stream radially towards the tank wall. Mao *et al*[9] reported the similar phenomenon in their experimental works. Additionally, the values of V_z for $T/3$ impeller, especially at the peaks, are overall higher and the peak positions are more close to the center of the tank.

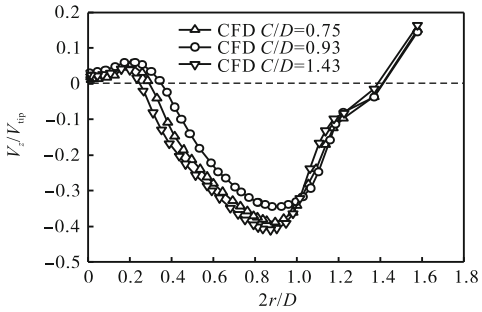

(a) C/D = 0.75 to 1.43

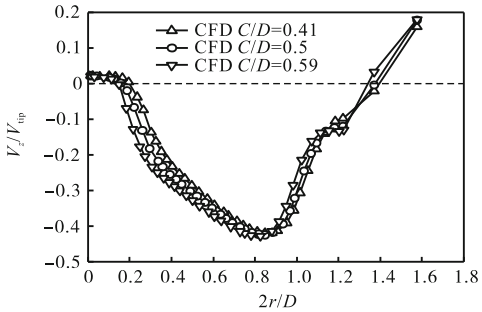

(b) C/D = 0.41 to 0.59

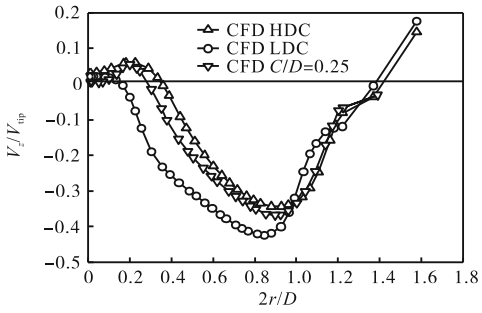

(c) Combined results

Fig. 8 Impeller discharge conditions for *T*/2 impeller

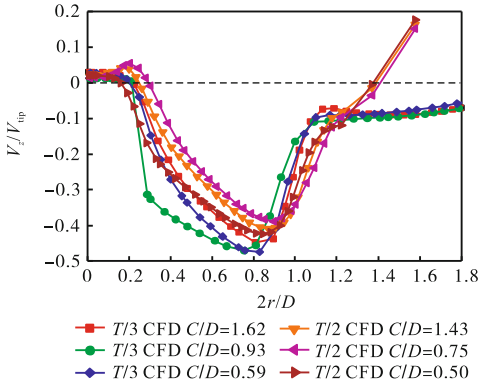

Fig. 9 Comparisons of V_z profiles of *T*/3 and *T*/2 impeller

2.4 Impeller pumping capacity

This section focuses on the effects of D and C on three macro-mixing indexes. Three predicted mixing parameters of $T/3$ and $T/2$ impeller were plotted against C/D.

In Fig. 10, N_p for $T/3$ impeller is high at low clearances and decreases almost linearly with increasing clearances until C/D reaches 1.43, which agrees well with the experimental results of Rewatkar *et al*[20]. Above C/D ratio of 1.43, N_p increases suddenly due to the transition of flow patterns. Then N_p tends to flat off and even has a slight decrease as C/D increases above 1.80. As for $T/2$ impeller, N_p has a similar trend to the $T/3$ impeller with increasing C/D, and the values of C/D at two inflection points on the curve are 0.75 and 1.25. A striking increase at $C/D = 0.75$ is also caused by the change of flow patterns. Additionally, N_p is overall higher for $T/3$ impeller.

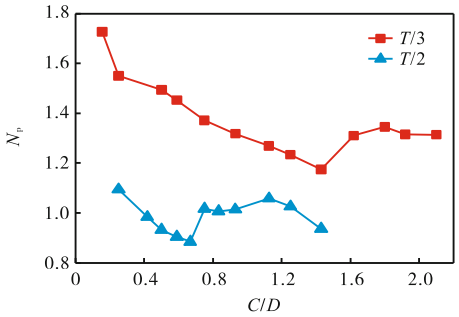

Fig. 10 Variations of N_p with C/D for $T/3$ and $T/2$ impeller

It can be concluded that P or N_p has a strong dependence on the flow fields or patterns. At the lowest C/D, the impeller discharge stream hits the bottom and has a sharp change in the flow direction, leading to much ineffective dissipation of energy and thereby the highest N_p. As C/D increases, strong impacts of the flow on the bottom decrease, thus the corresponding P and N_p decrease. When C/D increases to a certain value, the secondary circulation loop occurs below the impeller, which inhibits the impeller pumping action and thus N_p increases again. A decrease in N_p at $C/D = 1.80$ for $T/3$ impeller or $C/D = 1.25$ for $T/2$ impeller may be attributed to the dissipation of most kinetic energy during the flow paths and thus the inhibition of the secondary loop to the impeller action decreases.

The curves of N_{qp} versus C/D for two impellers are shown in Fig. 11. For $T/3$ impeller, N_{qp} increases steadily and then flats off until C/D increases to 0.93. Ranade and Joshi[6] also reported that N_{qp} for their standard impeller ($D = T/3$) increased with an increase of C/D if it was

less than 1. At low clearances, the proximity to the tank bottom makes the flow move radially outward to the wall. However, this 'bottom effect' decreases as C/D increases, and the peaks of V_z profiles increase and move towards the center of the tank (Fig. 7(d)), which indicates that more and more liquid is discharged toward the bottom from the impeller and thus N_{qp} increases. As C/D further increases above 0.93, a fraction of the impeller discharge stream begins to hit the tank wall again (Fig. 12). Therefore, N_{qp} begins to decrease and a transition of flow patterns begins to occur. N_{qp} has a dramatic increase at $C/D = 1.43$ just due to a complete transition of flow patterns. A dramatic change of N_{qp} at $C/D = 1.8$ is still found, which may be attributed to the proximity of liquid surface.

As for $T/2$ impeller, the curve of N_{qp} plotted against C/D is similar to that for $T/3$ impeller. The above reason can be used to explain the behavior of N_{qp} versus C/D. The values of C/D at two inflection points are still 0.75 and 1.25. In addition, N_{qp} for $T/2$ is smaller than that for $T/3$ impeller on the whole.

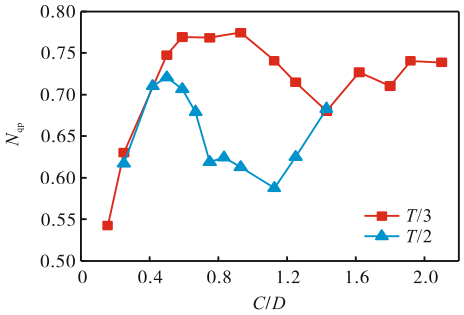

Fig. 11 Variations of N_{qp} with C/D for $T/3$ and $T/2$ impeller

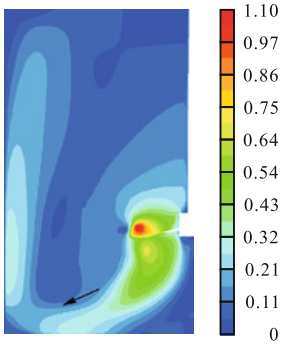

Fig. 12 Contours of liquid velocity for $T/3$ impeller when $C/D = 0.93$

Both N_p and N_{qp} for $T/3$ impeller are higher than those for $T/2$ impeller. Therefore, it is difficult to compare the pumping capacity between two impellers. Hence, another important index, η_e, is used to compare the effectiveness of the two impellers, and the results are shown in the form of η_e with respect to C/D (Fig. 13). The difference of the two curves is very clear. η_e for $T/2$ impeller becomes generally higher especially at lower C/D, which means $T/2$ impeller has a higher pumping rate given the same amount of power input.

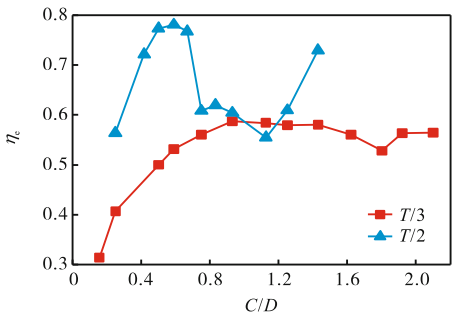

Fig. 13 Variations of η_e with C/D for $T/3$ and $T/2$ impeller

3 Conclusions

This work aimed to explore a CFD method to understand the macro-mixing characteristics including the mean flow field and impeller capacity produced by a 45° down-pumping pitched blade turbine in stirred tanks. The computational approach was based on RANS-based prediction along with realizable k-ε turbulence model, QUICK scheme and MRF approach. Three typical flow fields were described in detail, and effects of D and C on both the mean flow field and impeller capacity were then investigated.

As C/D increases, the transition of the "single-eight" flow pattern to the "double-eight" flow pattern occurs. The transition of flow patterns or the presence of secondary circulation loop depends strongly on D and C. As for $T/3$ impeller, the transition of the flow patterns occurs at C/D ratio around 1.43. As for $T/2$ impeller, the value of C/D at which the transition occurs is lower, around 0.75. The occurrence of the secondary loop below the impeller deflects the impeller discharge angle toward the horizontal.

Three global macro-mixing parameters (N_p, N_{qp} and η_e) were strongly affected by the mean flow fields. The behavior of three mixing parameters was analyzed at different C/D values, and dramatic changes were found when the secondary circulation loop formed. The values of C/D for the transition of flow patterns are the same as the above, and $T/2$ impeller has a higher pumping effectiveness than $T/3$ impeller.

References

[1] Ali A M, Yuan H H S, Dickey D S *et al*. Liquid dispersion mechanisms in agitated tanks (part I): Pitched blade turbine[J]. *Chemical Engineering Communications*, 1981, 10(4/5): 205-213.

[2] Khopkar A R, Aubin J, Xuereb C. Gas-liquid flow generated by a pitched-blade turbine: Particle image velocimetry measurements and computational fluid dynamics simulations[J]. *Industrial & Engineering Chemistry Research*, 2003, 42(21): 5318-5332.

[3] Sharma R N, Shaikh A A. Solid suspension in stirred tanks with pitched blade turbines [J]. *Chemical Engineering Science*, 2003, 58(10): 2123-2140.

[4] Chen J, Xiao W. Solids suspension study in a side-entering stirred tank through CFD modeling[J]. *International Journal of Chemical Reactor Engineering*, 2013, 11(1): 331-346.

[5] Aubin J, Mavros P, Fletcher D F *et al*. Effect of axial agitator configuration (up-pumping, down-pumping, reverse rotation) on flow patterns generated in stirred vessels[J]. *Chemical Engineering Research & Design*, 2001, 79(8): 845-856.

[6] Ranade V V, Joshi J B. Flow generated by pitched blade turbines I: Measurements using laser Doppler anemometer[J]. *Chemical Engineering Communications*, 1989, 81(1): 197-224.

[7] Rewatkar V B, Joshi J B. Effect of impeller design on liquid phase mixing in mechanically agitated reactors[J]. *Chemical Engineering Communications*, 1991, 102(1): 1-33.

[8] Kresta S M, Wood P E. The mean flow field produced by a 45° pitched blade turbine: Changes in the circulation pattern due to off-bottom clearance[J]. *Canadian Journal of Chemical Engineering*, 1993, 71(1): 42-53.

[9] Mao D, Feng L, Wang K *et al*. The mean flow field generated by a pitched blade turbine: Changes in the circulation pattern due to impeller geometry[J]. *Canadian Journal of Chemical Engineering*, 1997, 75(2): 307-316.

[10] Delafosse A, Line A, Morchain J *et al*. LES and URANS simulations of hydrodynamics in mixing tank: Comparison to PIV experiments[J]. *Chemical Engineering Research & Design*, 2008, 86(12): 1322-1330.

[11] Murthy N B, Joshi J B. Assessment of standard *k-ε*, RSM and LES turbulence models in a baffled stirred vessel agitated by various impeller designs[J]. *Chemical Engineering Science*, 2008, 63(22): 5468-5495.

[12] Aubin J, Fletcher D F, Xuereb C. Modeling turbulent flow in stirred tanks with CFD: The influence of the modeling approach, turbulence mode and numerical scheme[J]. *Experimental Thermal and Fluid Science*, 2004, 28(5): 431-445.

[13] Deglon D A, Meyer C J. CFD modelling of stirred tanks: Numerical considerations[J]. *Minerals Engineering*, 2006, 19(10): 1059-1068.

[14] Coroneo M, Montante G, Paglianti A *et al*. CFD prediction of fluid flow and mixing in stirred tanks: Numerical issues about the RANS simulations[J]. *Computers & Chemical Engineering*, 2011, 35(10): 1959-1968.

[15] Jaworski Z, Dyster K N, Nienow A W. The effect of size, location and pumping direction of pitched blade turbine impellers on flow patterns: LDA measurements and CFD predictions[J]. *Chemical Engineering Research & Design*, 2001, 79(8): 887-894.

[16] Rahimi M, Parvareh A. Experimental and CFD investigation on mixing by a jet in a semi-industrial stirred tank[J]. *Chemical Engineering Journal*, 2005, 115(1/2): 85-92.

[17] Ranade V V. *Computational Flow Modelling for Chemical Reactor Engineering*[M]. Academic Press, New York, 2002.

[18] Khazam O, Kresta S M. Mechanisms of solids drawdown in stirred tanks[J]. *Canadian Journal of Chemical Engineering*, 2008, 86(4): 622-634.

[19] Chen T, Wang L, Wu D *et al.* Investigation of the mechanism of low-density particle and liquid mixing process in a stirred vessel[J]. *Canadian Journal of Chemical Engineering*, 2012, 90(4): 925-935.

[20] Rewatkar V B, Raghava K S M S, Joshi J B. Power consumption in mechanically agitated contactors using pitched bladed turbine impellers[J]. *Chemical Engineering Communications*, 1990, 88(1): 69-90.

(Editor: Zhao Yang)